

#### **PAPER • OPEN ACCESS**

# Real-time motion modeling and treatment verification for irregular motion in carbon ion therapy: a feasibility study

To cite this article: C Galeone et al 2025 Phys. Med. Biol. 70 165009

View the article online for updates and enhancements.

#### You may also like

- Time-resolved dynamic CBCT reconstruction using prior-model-free spatiotemporal Gaussian representation (PMF-STGR)
  Jiacheng Xie, Hua-Chieh Shao and You Zhang
- New Geant4-DNA physics model for electron track-structure simulations in gold nanoparticles loannis Polopetrakis, loanna Kyriakou, Dousatsu Sakata et al.
- A DCT-UNet-based framework for pulmonary airway segmentation integrating label self-updating and terminal region growing Shuiqing Zhao, Yanan Wu, Jiaxuan Xu et al





Increase your workflow efficiency without sacrificing quality.



Maximize your measurement accuracy and precision.



Have confidence in the QA software trusted among top treatment facilities.

**CLICK TO LEARN MORE** 

For over 32 years, RIT has provided medical physicists with an impressive range of convenient QA software packages to fit both your needs and budget. The RIT Family of Products software provides patient, machine, and imaging QA for TG-142, TG-148, TG-135, as well as automated phantom analysis for diagnostic imaging. RIT software utilizes a combination of powerful, robust routines in a user-friendly interface to maximize the efficiency and precision of your measurements. Easily export your analysis data as customizable reports or to the RIT $trend^{\text{TM}}$  statistical database for large-scale tracking and trending over time.

Visit radimage.com to find your perfect QA software solution today.

Email: sales@radimage.com

Call: 1(719) 590 - 1077, Opt. 4

©2025, Radiological Imaging Technology, Inc.

### Physics in Medicine & Biology





#### **OPEN ACCESS**

#### RECEIVED

1 April 2025

REVISED

14 July 2025

ACCEPTED FOR PUBLICATION 29 July 2025

PUBLISHED

11 August 2025

Original content from this work may be used under the terms of the Creative Commons Attribution 4.0 licence.

Any further distribution of this work must maintain attribution to the author(s) and the title of the work, journal citation and DOI.



#### **PAPER**

## Real-time motion modeling and treatment verification for irregular motion in carbon ion therapy: a feasibility study

C Galeone<sup>1,2,3,11,\*</sup>, A Nakas<sup>4,11</sup>, M Donetti<sup>5</sup>, M C Martire<sup>1,2</sup>, F M Milian<sup>6,7</sup>, A Pella<sup>8</sup>, C Paganelli<sup>4</sup>, R Sacchi<sup>3,6</sup>, A Vignati<sup>3,6</sup>, M Durante<sup>1,9,10</sup>, G Baroni<sup>4,8</sup>, S Giordanengo<sup>6</sup> and C Graeff<sup>1,2</sup>

- Biophysics, GSI Helmholtzzentrum für Schwerionenforschung, Darmstadt, Darmstadt, Germany
- <sup>2</sup> Department of Electrical Engineering and Information Technology, TU Darmstadt, Darmstdt, Germany
- Department of Physics, Università degli Studi di Torino, Torino, Italy
- Department of Electronics, Information and Bionengineering, Politecnico di Milano, Milano, Italy
- <sup>5</sup> Research department, CNAO Centro Nazionale di Adroterapia Oncologica, Pavia, Italy
- <sup>6</sup> Istituto Nazionale di Fisica Nucleare, Torino, Torino, Italy
- Universidade Estadual de Santa Cruz, Ilheus, Brazil
- <sup>8</sup> Bioengineering Unit, CNAO Centro Nazionale di Adroterapia Oncologica, Pavia, Italy
- <sup>9</sup> Institute for Condensed Matter Physics, TU Darmstadt, Darmstadt, Germany
- Department of Physics, Università Federico II, Napoli, Italy
- Both authors share first authorship.
- \* Author to whom any correspondence should be addressed.

E-mail: c.galeone@gsi.de

Keywords: real-time dose calculation, particle therapy, irregular motion, motion model, adaptive therapy

#### **Abstract**

Objective. Irregular motion impacts treatment accuracy and can be compensated by larger margins or online adaptive approaches. A seamless workflow for fast and accurate 4D-dose reconstruction allows dosimetric monitoring intra- and inter-fractionally, as a basis for adaptive therapy. This study presents a real-time, motion-adaptive framework that combines motion modeling and treatment verification, integrated into the dose delivery and monitoring systems to enable continuous assessment of the delivered 4D-dose. Approach. The framework includes a GPU-based analytical algorithm for real-time dose reconstruction in carbon ion therapy, interfaced with the dose delivery and optical tracking systems at the Centro Nazionale di Adroterapia Oncologica (CNAO). A motion model, driven by external surrogate tracking, generates a virtual CT every 150 ms, used for 4D-dose reconstruction with measured spot parameters. Planned and delivered doses are compared after each iso-energy slice. The framework was validated at CNAO using a geometric target and a 4D lung tumor phantom with a moving 2D ionization chamber array, under regular and irregular motion patterns. Main results. The framework successfully generated real-time CT images of the lung phantom, showing strong agreement with ground-truth images. Dose reconstructions were performed within inter-spill times during delivery, ensuring rapid assessment. Comparisons against detector measurements yielded an average gamma-index passing rate of 99% (3%/3 mm), confirming the accuracy of both the motion model and the integrated treatment verification system. Significance. This work presents the first real-time framework for carbon ion therapy, integrating motion modeling and dose reconstruction to handle irregular motion, fully embedded in a clinic-like setup.

#### 1. Introduction

Cancer remains one of the leading causes of morbidity and mortality worldwide, with radiotherapy being a cornerstone in its treatment (Lawler *et al* 2023). Traditional radiotherapy employs electrons or x-rays to target and destroy malignant cells, but its efficacy is limited by the inevitable damage to surrounding healthy tissues (Sanford *et al* 2019). To address these limitations, particle therapy has emerged as a highly precise

alternative, leveraging the unique biological and physical properties of heavy ions (Durante and Loeffler 2010).

However, the success of particle therapy is significantly challenged by range uncertainty (Lomax 2020) and the dynamic nature of tumors in the abdominal/thoracic area (Bert and Durante 2011). Tumors can shift due to respiration (Yoganathan *et al* 2017) or change size and shape (Barker *et al* 2004), causing misalignment of beam and target that potentially reduces tumor dose and increases dose to surrounding tissues (Bert *et al* 2008). Motion management is vital to account for and compensate for such variations (Pakela *et al* 2022).

Different motion mitigation strategies, such as gating (Ciocca *et al* 2016), rescanning (Grassberger *et al* 2015), and multi-phase 4D (MP4D) (Lis *et al* 2020, Steinsberger *et al* 2023), have been proposed to handle patient motion, reducing the interplay effect. However, their reliance on a 4D computer tomography (4DCT) may not capture anatomic changes occurring in-between fractions (inter-fraction) (Den Otter *et al* 2020). To this extent, online daily adaptive therapy proposes a new workflow by acquiring a new image of the patient before the daily fraction to update the plan (Albertini *et al* 2024). Nonetheless, these approaches remain susceptible to intra-fractional motion, like target drifts and variable breathing patterns (Dhont *et al* 2018).

For conformal compensation of intra-fraction motion, beam tracking (Riboldi *et al* 2012) and MP4D with residual tracking (Steinsberger *et al* 2023) were proposed, but are still not in clinical use.

Regardless of the adopted approach, online treatment verification is crucial to judge the efficacy of motion mitigation measures. Several procedures have been proposed based on secondary radiation (Parodi *et al* 2023, Werner *et al* 2024), and machine log-files (Choi *et al* 2018, Meijers *et al* 2019). Among the latter, some reconstructions consider motion irregularities (Duetschler *et al* 2023, Steinsberger *et al* 2021), but they are performed retrospectively.

A solution to assess arbitrary motion online is global motion models (Fassi *et al* 2015, Nakas *et al* 2024), which provide continuous time-resolved 3D anatomical information. These models integrate 4D imaging with surrogate-based data acquired during delivery to predict and generate dynamic 3D volumes representing the patient's anatomy of the moment. Although less accurate than direct imaging methods such as continuous kV imaging, model-based approaches offer reduced imaging dose, low latency, and continuous tracking even during beam-off times (Bertholet *et al* 2019). Hybrid approaches using sparse imaging together with surrogate signals are already used clinically in conventional radiotherapy (Matsuo *et al* 2014).

Both inter- and intra-fractional adaptive methods require an integrated tool for 4D dose assessment (Trnkova *et al* 2023, Zhang *et al* 2023). RIDOS (Giordanengo *et al* 2019) and 4D-RIDOS (Galeone *et al* 2024) are examples of such software, enabling the reconstruction of planned and delivered doses during treatment and providing prompt feedback on quality within the inter-spill time of synchrotron-based facilities. This system is already integrated into the 4D research version of the dose delivery system (4D-DDS) (Lis *et al* 2020, Steinsberger *et al* 2023, Donetti *et al* 2021) at CNAO (Italy), with experimental results confirming its accuracy in regular 4D motion scenarios (Galeone *et al* 2024).

We propose a dedicated framework to manage motion integrating a global motion model, to provide concurrent real-time treatment verification for 4D (regular) and 5D (irregular) motion scenarios. The input for the motion model is received through an abstract interface to the DDS, with the data in this study provided by optical tracking of external surrogates. The internal anatomy is reconstructed within an extended version of the fast forward dose calculation (FDC) tool (Giordanengo *et al* 2019, Galeone *et al* 2024), called 5D-RIDOS, which also performs real-time treatment validation. The seamless integration of the CNAO optical tracking system (OTS), 4D-DDS, and 5D-RIDOS represents a fully automated framework for real-time feedback on treatment quality without additional input from clinical staff, significantly reducing workload—an essential feature for adaptive therapy settings.

A comprehensive description of the framework's hardware and software configuration is given along with the results of its experimental validation performed at CNAO.

#### 2. Materials and methods

#### 2.1. Motion model and virtual time-resolved CT generation

Our framework leverages a pre-existing external-internal correlation model (Fassi *et al* 2015), adapted for real-time execution during delivery. In brief, the model is based on the mid-position (midP) CT, a time-averaged position over the planning 4DCT, and deformable vector fields (DVFs), which link the same voxels from the midP CT to the planning anatomy of the patient.

During delivery, the tracked motion trace is compared with the planned motion, and a Hilbert transform is applied to extract instantaneous phase and amplitude parameters. These two are used to interpolate the DVFs: the instantaneous phase identifies which DVF pairs to interpolate (e.g. between phase 0 and 1), while the amplitude rescales the deformation magnitude. This results in a new deformation field applied to the

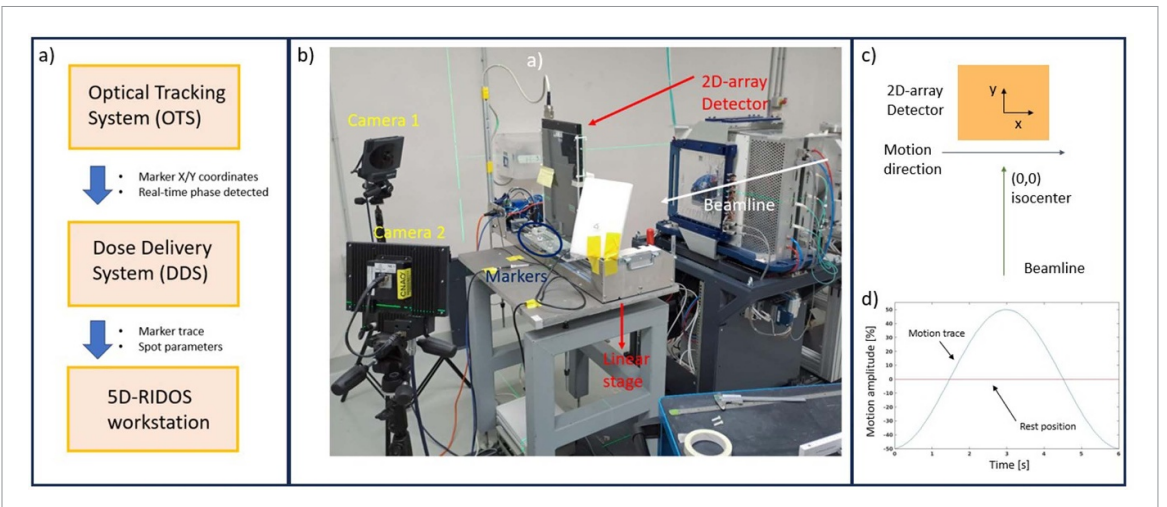


**Figure 1.** (a) Schematic view of the connection between OTS, 4D-DDS, and the 5D-RIDOS workstation. (b) Picture of the experimental setup at CNAO's experimental room. (c) Schematic view of the 2D-array detector orientation compared to the beamline. The rest position of the detector is at the isocenter, and it moves 1D towards negative and positive *x*-coordinates, as represented in (d).

midP CT, enabling real-time generation of a virtual CT representing the anatomy of the patient. A graphical representation of the motion model is provided in appendix A.

#### 2.2. OTS—4D-DDS—5D-RIDOS connections

The DDS at CNAO includes a control system that oversees beam delivery during patient treatments (Giordanengo *et al* 2015). A modified research version, enabling 4D delivery (4D-DDS) and currently under CE approval, was previously outlined (Lis *et al* 2020, Steinsberger *et al* 2023, Donetti *et al* 2021).

The OTS consists of a commercial system (SMART-DX100, BTS Bioengineering, Garbagnate, Italy) equipped with two infrared cameras and custom in-house software to perform real-time motion monitoring (Fattori *et al* 2014). The system was used to capture the in-plane position of a marker, at a frame rate of 70 Hz with post-calibration sub-millimeter accuracy (~0.5 mm).

The communication between OTS and 4D-DDS has been established with a digital I/O module (Sealevel Systems, South Carolina, US), to transmit the motion data, *X/Y* marker position and detected phase, via a custom Modbus TCP/IP protocol.

Dedicated tests assessed delay contributions from OTS data transfer to the 4D-DDS. The OTS was benchmarked against a Gefran PZ-12-S-150 position transducer by tracking a sliding table in sinusoidal motion (4 s period). Motion data from both systems were synchronized at 1 kHz, and the phase shift between signals quantified the processing and communication delay.

5D-RIDOS (Giordanengo *et al* 2019, Galeone *et al* 2024) was updated to receive the OTS-derived motion trace and raw dose delivery data from the 4D-DDS, generated after each spot or every 50 ms during beam off, by means of a TCP/IP protocol. A schematic view of the connection between components (OTS—4D-DDS—5D-RIDOS workstation) is represented in figure 1(a).

#### 2.2.1. Experimental setup

The testing of our framework was conducted at CNAO's experimental room, equipped with a horizontal beamline and the 4D-DDS. The experimental setup mimics a quality assurance arrangement, with an ionization chamber (IC) 2D-array (PTW Octavious 1500XDR, PTW, Freiburg, Germany) mounted on a linear stage moving perpendicular to the beamline, figure 1(b). Plates of polymethyl methacrylate (PMMA) or of solid water were placed in front of the detector to maximize the high dose region recorded. Different water equivalent thicknesses were used according to the specific plan delivered.

The OTS observed the detector's motion, simulating a moving patient, by tracking three markers placed on the linear stage's surface. Only the coordinates of the most stable and least noisy marker were transmitted to the 4D-DDS. Additionally, the OTS performed phase binning and streamed the phase and *X/Y* marker coordinates (perpendicular to the beamline) to the 4D-DDS.

The rest position of the detector was aligned at the isocenter, as in figure 1(c), with a symmetric motion, figure 1(d). There was residual uncertainty over the correct alignment between the rest position and the isocenter. A static plan without motion was delivered to the detector and was used to correct the setup error in all following deliveries.

The linear stage was programmed to move regularly and irregularly. The regular cases were conducted with an amplitude ranging between 18.7 and 21 mm (maximum exhale–maximum inhale) and a fixed, per delivery, period of 5–6 s. For the irregular cases, the period was kept fixed during the treatment, however amplitude variations and baseline drifts were considered.

#### 2.3. 5D-RIDOS

#### 2.3.1. Workflow

The structure of 5D-RIDOS resembles the one previously described in Giordanengo *et al* (2019) and Galeone *et al* (2024). The system uses a graphical user interface (GUI), developed in MATLAB (2018b), handling the connection to the 4D-DDS and to the FDC, developed in CUDA (Vingelmann and Fitzek 2022), for the dose calculation.

Before treatment, the system requires some input parameters such as the midP CT, the treatment plan, and the DVFs—the motion model to describe the patient's irregular anatomy during delivery is built *a priori*.

The real-time parameters required by the FDC are provided by the GUI, after translating the raw data received by the 4D-DDS. In particular, the system needs the spot parameters, specifically the beam energy, its position and number of particles measured by the beam monitors, along with the instantaneous phase and amplitude used to generate a new CT.

To limit residual motion and to properly capture the impact of irregular motions, the GUI triggers a new calculation at a fixed rate 'triggering window', if at least one spot was delivered within this time window, as well as at the end of an energy slice. It first applies the Hilbert transform to the planned and delivered motion signals to generate the instantaneous phase and amplitude used for the CT generation by the FDC. The delivered dose is then reconstructed on the new anatomy of the patient, warped back on the midP CT, and at the end of the energy slice the data are transferred to the GUI for display.

The GUI also loads the planned dose, calculated beforehand, and runs an independent GPU-based gamma-index comparison (Persoon *et al* 2011) of planned versus delivered dose up to that point. Finally, the results are reported on the screen.

For a graphical illustration of the described workflow, refer to appendix B.

#### 2.3.2. Dose reconstruction algorithm

The FDC consists of a pencil-beam algorithm (Russo *et al* 2015) and it relies on the interpolation of pre-computed look-up tables (LUTs) and a raytracing algorithm (Siddon 1985). To keep the reconstruction in real-time, the dose engine has been implemented on GPU, exploiting parallel computing, as already presented by Giordanengo *et al* (2019) and Galeone *et al* (2024).

Compared to the previous versions, the beam propagation algorithm has been renovated. The FDC identifies the voxels within a certain cutoff to handle the beam spread. This step does not consider the density of lateral voxels, which are assumed to be water. 5D-RIDOS applies a grid mask around the beam axis to significantly limit the search volume and memory consumption. The grid size can be set by the user, with up to  $31 \times 31$  voxels placed symmetrically around the beam propagation axis. This version of the algorithm permits reconstructing the dose for particle arc therapy deliveries (Mein *et al* 2024). It would not have been possible with the previous version of the algorithm because of memory issues (Galeone *et al* 2024), and too time-consuming with the original version (Giordanengo *et al* 2019).

Moreover, the FDC interpolates the supplied DVFs with the instantaneous phase and amplitude and warps the midP CT to generate the new anatomy of the patient. The dose is then reconstructed on it, and warped back to midP CT and sent to the GUI for display at the end of each iso-energy slice.

In contrast to the previous version of the algorithm, 5D-RIDOS only performs the reconstruction of the delivered dose, while the planned dose, computed before the delivery, is directly loaded by the GUI slice by slice.

#### 2.4. Experimental validation of the framework

The main goals of this experiment were to check the accuracy of the algorithm to reconstruct the CT, precision and time performance of the system, and finally to assess the sensitivity of such a system in case of irregular motions compared to conventional 4DCT-based dose reconstructions.

#### 2.4.1. Treatment plans

The experimental tests involved delivery of multiple plans optimized using TRiP98 (Steinsberger *et al* 2021, Richter *et al* 2013), on a water cube and on a virtual four-dimensional extended cardiac-torso (XCAT) (Steinsberger *et al* 2023, 2021, Segars *et al* 2008).

The XCAT phantom and its applications are reported in more detail in Steinsberger *et al* (2021). For our study, 10 out of 25 generated 4DCT phases were selected, covering half a respiratory cycle from maximum

inhale to maximum exhale. The patient features a spherical tumor in the left lung, exhibiting a phase-stepped motion of 40 mm in the cranio-caudal (CC) direction and 20 mm in the anterior-posterior direction. The 10 selected phases describe a tumor motion amplitude of 19.8 mm in CC, with the end-exhale CT set as reference. Some of the non-selected phases were used to test the motion model's ability to generate new CTs. The tumor's center of mass (COM) was used as marker position, establishing a direct one-to-one correlation between the target-marker motions.

For the XCAT, four posterior plans have been optimized: range-ITV (Graeff 2014), MP4D, gating (gating window  $\pm 40\%$  around reference phase), and a 3D plan on the reference phase, all delivered under different conditions. The range-ITV, MP4D, and 3D plans were delivered with the linear stage moving regularly, while the gating plan was also tested with irregular detector motion. This specific scenario was selected for the irregular motion study as gating represents one of the most clinically adopted strategies for motion management (Zhang *et al* 2023), making it a particularly relevant case for assessing the framework's applicability in routine practice.

For the water cube, two different plans have been generated: a 2D-square and a cube MP4D, considering the tumor motion as animated on the 4DCT of the XCAT. The 2D-square and the cube MP4D plan have been delivered with regular and irregular motions.

#### 2.4.2. CT reconstruction algorithm benchmark

The benchmark of the CT reconstruction algorithm has been conducted on the XCAT phantom, exploiting some of the non-selected 4DCT phases, out of the 25 available in total. For this *in-silico* test, we adopted the tumor's COM as marker position, with a one-to-one correlation between the target-marker motions.

The model starts with the planning 4DCT and the planning signal generated as the target's COM in the 10 phases of motion. Three different 'delivery' scenarios were generated, characterized by different motion amplitudes: nominal higher (23.1 mm), nominal planning (19.8 mm), and nominal lower (14.8 mm), each representing the COM displacement between maximum end-exhale and maximum inhale. While the nominal planning scenario corresponds to the planned motion, the nominal higher/lower amplitudes were produced by exploiting other XCAT phases out of the 25 available, simulating two irregular breathing cycles. The comparison between the Hilbert transform of the planned and observed motion resulted in the instantaneous phase and amplitude parameters used to generate the new anatomies from the midP CT.

The newly generated CTs were compared against the ground truth ones, computing the Hausdorff distance between the generated and nominal target VOIs with Plastimatch. Additionally, the COM of the generated CTs was compared against the COM of the real XCAT anatomy.

These tests are not intended to validate the motion model itself, which has already been thoroughly validated (Fassi *et al* 2015), but rather to verify the correct implementation of the model within our framework.

#### 2.4.3. Dose calculation accuracy assessment

The dose calculation accuracy assessment has been conducted by comparing the 5D-RIDOS reconstructed doses against the detector measurements. Commissioning data for the beamline of the experimental room of CNAO was used to generate 3D LUTs for dose calculation.

The doses have been calculated on a homogeneous water cube  $[200 \times 200 \times 200, 1 \text{ mm}^3 \text{ voxel size}]$ , and the agreement against the detector was evaluated with a gamma-index analysis with 3%/3 mm and 2%/2 mm criteria.

Moreover, the calculation for all deliveries has been conducted with multiple triggering windows to generate a new virtual CT: 150 ms, 300 ms, and 500 ms. The study aims to understand the impact of the residual motion on the agreement between the reconstructed doses and the detector measurements.

For the dosimetric assessment of 5D-RIDOS against the detector measurement, the motion model was built from the mean motion trace derived from the first acquisition of the detector's motion, acting as the planning respiratory signal binned in 10 phases (figure 2). The planning 4DCT was represented by the displacement of the detector with respect to the reference phase (end-exhale).

The midP CT was defined as the rest position of the CT, which coincides with the time-averaged position, and registered to all the 10 binned phases of the motion (figure 2). The DVFs, rigidly mapping the midP CT to the 10 phases of the detector motion, have been generated for the motion model and dose reconstruction.

To show the improved accuracy when irregular motion is considered, doses have also been reconstructed using the previous 4D-RIDOS algorithm, that is by binning all beam spots to the phases of a regular, periodic 4DCT, as is the case for the majority of the log file-based dose reconstruction algorithm.

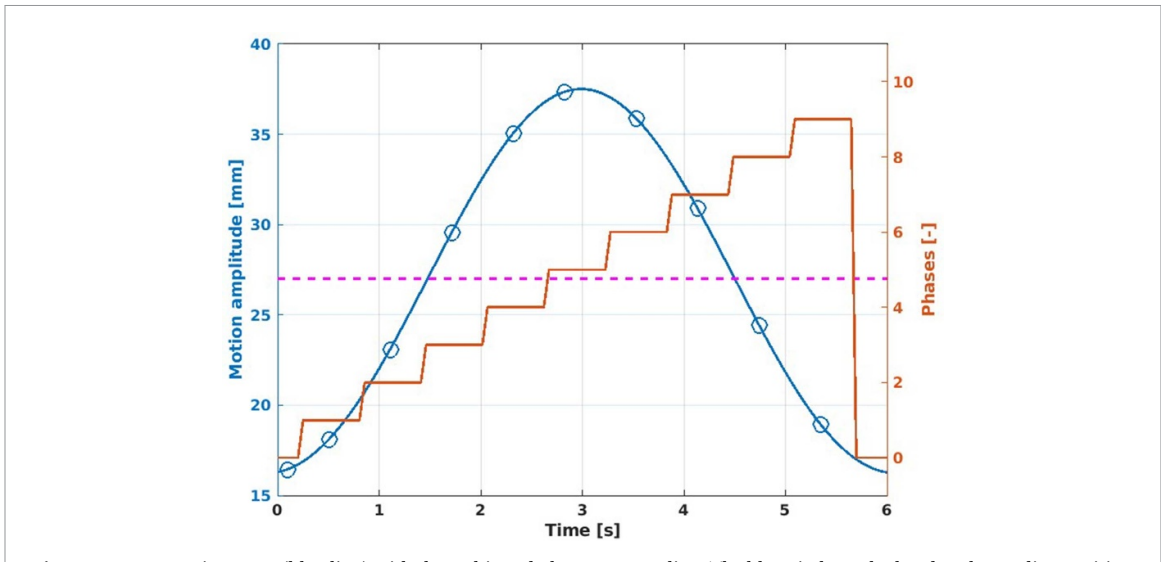


**Figure 2.** Mean motion trace (blue line) with the 10 binned phases, orange line. The blue circles, calculated as the median position of the marker in each phase, have been used to generate the DVFs. In purple the rest position of the detector at the isocenter.

#### 2.4.4. Processing time evaluation

The ultimate goal of 5D-RIDOS is to provide feedback on the accuracy of the delivery within the beam pause of the synchrotron. The accuracy of the reconstruction and the processing time have been evaluated for all deliveries, including the 150 ms triggering window only, as this is the most time-critical setting.

In particular, the time interval between the reception of the end-of-slice event from the DDS and the moment the GUI receives back the reconstructed dose from the FDC has been measured. This includes not only the 5D-RIDOS calculation time spent to perform the reconstruction but also the time the GUI takes to first apply the motion model, send the data to the FDC, and receive back the reconstructed dose.

The measurements have been conducted with a MATLAB *built-in* function, with a time resolution of 1 ms.

#### 3. Results

The delay of data transmission from the OTS to 4D-DDS (section 2.2) was assessed to be 30 ms, much shorter than the smallest triggering window of 150 ms. The setup measurement of the static dose distribution resulted in a lateral shift of 1 mm, which was applied to all dose reconstructions.

#### 3.1. CT reconstruction algorithm benchmark

The benchmark of the algorithm for the CT reconstruction has been conducted by comparing the generated CTs against the original XCAT ones. In particular, the average and maximum Hausdorff distance have been calculated (table 1) for the three different scenarios: nominal higher amplitude, nominal planning amplitude, and nominal lower amplitude. Moreover, the COM of the generated CTs has been compared with the original one, as depicted in figure 3.

From figure 3, it is possible to appreciate how the COM of the target follows the nominal one for all three scenarios. The discrepancy between the COM of the generated CTs and the nominal ones was on average of 0.46 mm and at most 1.06 mm, for phase 8 of the nominal lower amplitude case.

The Hausdorff distance expresses a good agreement between the results of the motion model and the original XCAT CTs, with a maximum average of 0.63 mm for the nominal lower amplitude scenario, relative to the same phase presenting the maximum discrepancy of the COM. This comparison shows the accuracy of the motion model, in agreement with Fassi *et al* (2015), and it represents the base of the 5D dose reconstruction performed by the algorithm.

#### 3.2. Dose calculation accuracy assessment

The agreement between reconstructed and measured doses is reported in table 2.

While the average results improve for shorter triggering windows, the difference is small and likely not clinically relevant for most cases. The only exceptions are the 2D-square plans, for regular and irregular scenarios. The reconstruction of the dose for such cases is of particular complexity for pencil beam

e reports also

**Table 1.** Average boundary and maximum Hausdorff distance between planned and generated VOIs for the three delivery scenarios: nominal higher amplitude, nominal planning and nominal lower amplitude. The table reports also the distance between the planned and generated center of mass (COM) of the target VOI. Bold values highlight the maximum discrepancy observed across all scenarios and phases.

	Nominal higher amplitude CTs				Nominal planning CTs	}	Nominal lower amplitude CTs		
Phase	Avg boundary HD (mm)	Max boundary HD (mm)	ΔCOM (mm)	Avg boundary HD (mm)	Max boundary HD (mm)	ΔCOM (mm)	Avg boundary HD (mm)	Max boundary HD (mm)	ΔCOM (mm)
0	0	0	0	0	0	0.01	0.41	0.42	0.78
1	0.38	0.39	0.19	0.58	0.58	0.98	0.25	0.25	0.42
2	0.41	0.42	0.43	0.29	0.31	0.12	0.19	0.2	0.11
3	0.48	0.49	0.22	0.15	0.16	0.25	0.33	0.33	0.52
4	0.36	0.36	0.51	0.42	0.43	0.44	0.29	0.29	0.44
5	0.46	0.47	0.78	0.39	0.41	0.36	0.39	0.4	0.77
6	0.56	0.57	0.92	0.25	0.25	0.32	0.51	0.51	0.9
7	0.48	0.48	0.84	0.29	0.3	0.13	0.29	0.29	0.51
8	0.28	0.28	0.5	0.38	0.39	0.8	0.63	0.63	1.06
9	0.25	0.25	0.12	0.19	0.19	0.21	0.17	0.17	0.2

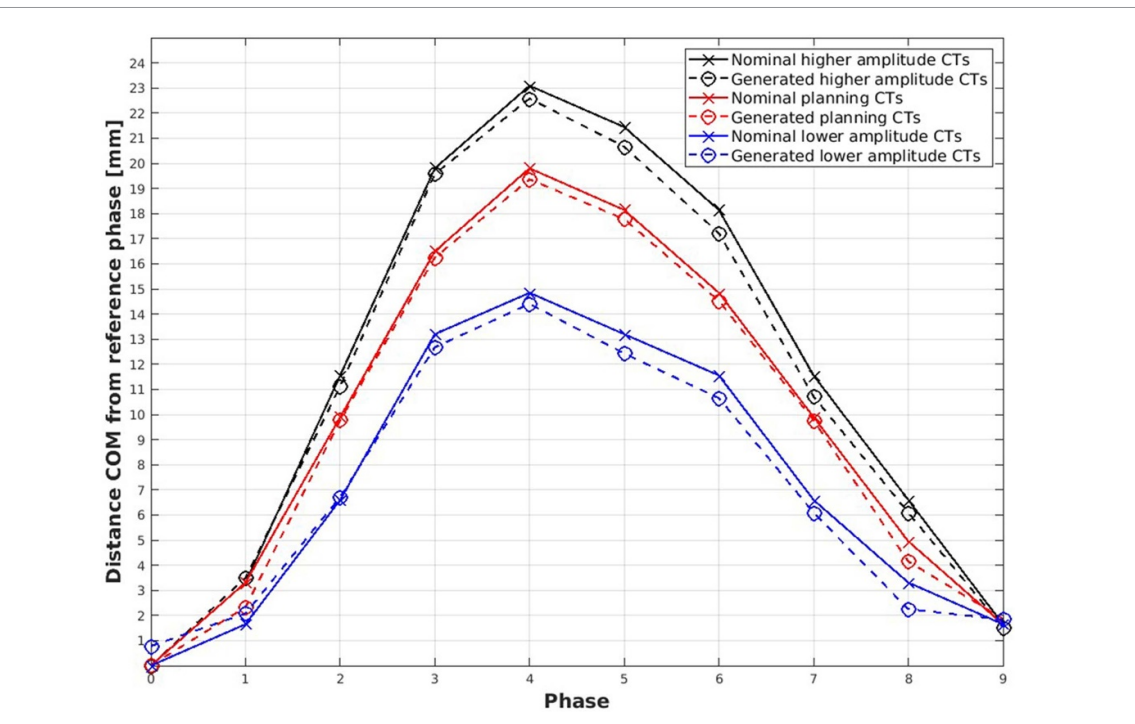


Figure 3. Center of mass (COM) of planned and generated target VOI for the three delivery scenarios: nominal higher amplitude (black), nominal planning (red), and nominal lower amplitude (blue). The nominal COMs are the continuous lines with crosses, while the generated COMs are the dashed lines with circles.

algorithms. A 2D plan is characterized by a limited number of spots, less than 1000 in our case, with a high weight (1 million particles) leading to significant interplay effect.

Due to the limited averaging in this single energy delivery, the residual motion within the larger time frames lead to reduced accuracy, as it can be appreciated in figure 4. Only deliveries with 5D-RIDOS and 150 ms triggering window show a gamma-index passing rate >95% at 3%/3 mm for all studied modes. The use of regular 4DCTs results in consistently smaller gamma values, especially for irregular motion. This effect is mitigated by the inherent rescanning of MP4D, which also compensates for irregular motion.

A representative example of this comparison comes from a gated delivery with the detector moving irregularly, see figure 5. The gamma-index passing rate (3%/3 mm) of the 5D-RIDOS reconstructed dose is of 100%, while 4D-RIDOS shows relevant deviations from the measurement. The 4DCT-based method proved to be accurate enough for most of the regular motion deliveries, except the 2D-square plans, due to the impact of the residual motion, as reported in table 2.

For all use cases, 5D-RIDOS, especially with a short triggering window, outperformed the 4D-RIDOS approach. This is connected to the residual motion within each motion phase or triggering window: the mean motion within a 4DCT phase is 4.2 mm, while it is close to 1 mm within the 150 ms window, see table 3. Despite a comparable residual motion between the 4DCT-based approach and the 500 ms triggering window, the latter is more precise for the irregular motion cases (table 2).

The number of CTs generated per delivery depends on the treatment delivery duration and the size of the triggering window. It varies between the 2D-square plan and MP4D, where more than 1000 CTs per treatment can be required. The residual motion increases with the size of the triggering time window, remaining however smaller than what is obtained from the 4DCT-based approach.

The measured residual motion is also affected by the motion period of the detector. For example, the cube MP4D plans have been delivered with a period of 6 s, as well as those for XCAT, thus reducing the residual motion compared to the square plans (5 s period). This effect is particularly emphasized for the 500 ms triggering window.

#### 3.3. Processing time evaluation

The processing time has been evaluated as the interval between the end of the energy slice event received by the 4D-DDS and when the GUI receives the reconstructed dose, ready to be displayed, as captured in figure 6. The recorded spots are labeled as red crosses, the 4D-DDS event of the end of energy slice is in purple and the green line represents the reception of the reconstructed dose by the GUI. It can be appreciated how the dose is updated right after the end of the energy slice end, leaving sufficient time to perform the

ر رغام

**Table 2.** Results of gamma-index comparison between reconstructed doses and detector measurements for three different triggering time windows: 150, 300 and 500 ms, and for the 4DCT-based approach. The reported average gamma-index criteria are 3%/3 mm and 2%/2 mm. N represents the number of deliveries per type.

		4DCT-based	Trigger 150 ms	Trigger 300 ms	Trigger 500 ms	Trigger 150 m	Trigger 300 ms	Trigger 500 ms	
Plan	N	Gamma (3%/3 mm)				(2%/2 mm)			
2D-square (regular)	3	92.5	97.5	94.1	91.7	78.4	81.2	76.6	
2D-square (irregular)	2	89.2	96.2	96	92.8	84.4	84.2	83.4	
Cube MP4D (regular)	2	99.3	99.5	99.6	99.5	96.9	97	97.3	
Cube MP4D (irregular)	3	99.9	100	100	99.9	96.7	96.6	96.2	
XCAT (regular)	11	97.9	99.5	99.1	99.3	96.5	95.2	94.9	
XCAT (irregular)	1	92.7	100	99.1	99.6	96.1	95.2	95.2	
Mean		96.8	99	98.3	98	94.2	92.7	92.5	

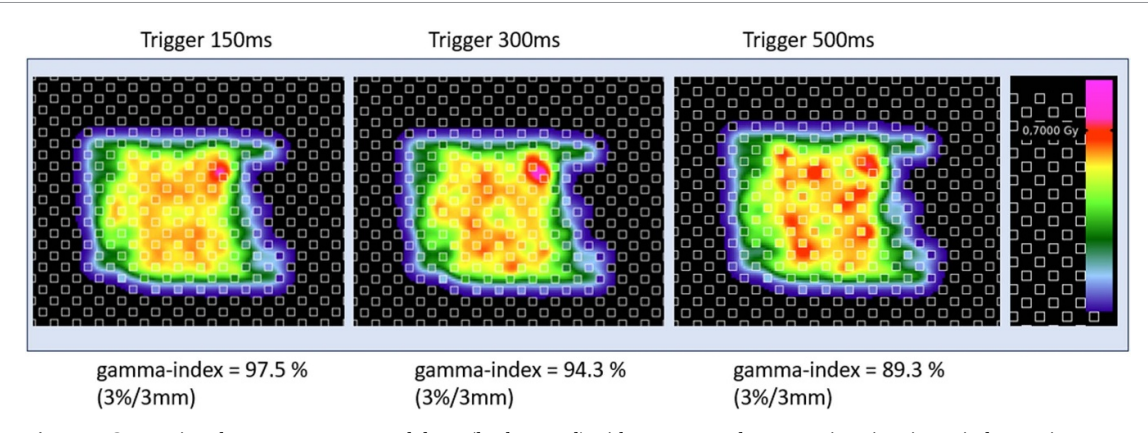


**Figure 4.** Comparison between reconstructed doses (background) with 150, 300 and 500 ms triggering time window against detector measurements (within the white boxes). The reported doses are from the horizontal profile, perpendicular to the propagation axis. The image refers to a 2D-square interplay delivery with regular motion of the detector. There was no bolus in this delivery, therefore the images refer to the entrance channel of the water box used for the reconstruction.

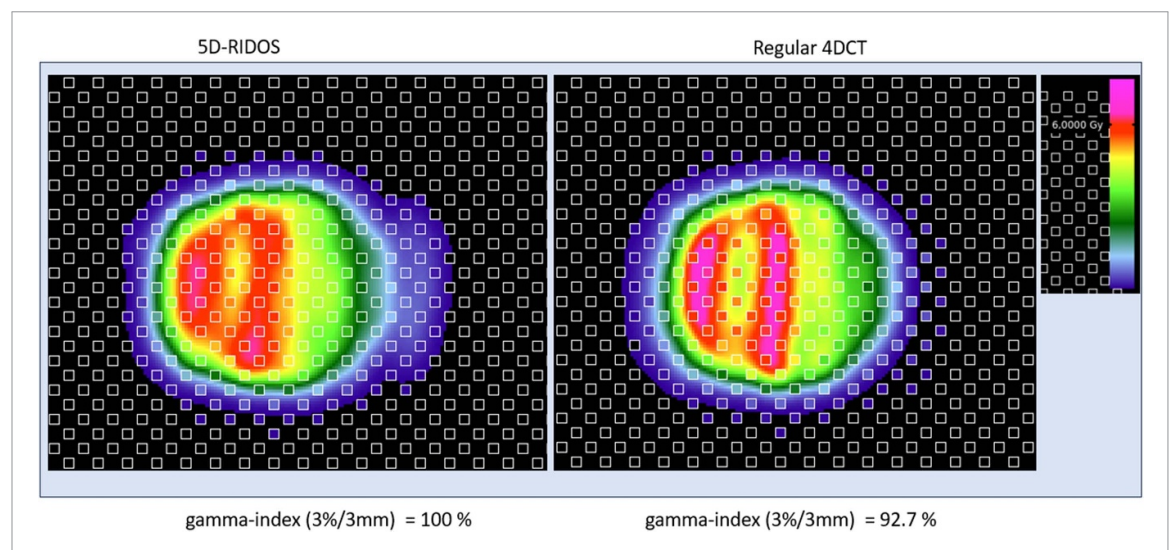


**Figure 5.** Comparison between reconstructed doses by 5D-RIDOS (left side) and 4DCT-based approach (right side). The reconstructed doses are in the background, the detector measurement in the white boxes. The image refers to a gating delivery with irregular motion of the detector.

**Table 3.** Comparison between number of generated CTs and residual motion for the three triggering time windows tested: 150, 300 and 500 ms.

	Mear	n # of CTs gen	erated	Resid	Residual motion (mm)		
Triggering window:	150 ms	300 ms	500 ms	150 ms	300 ms	500 ms	
2D-square (5 s period)	124	67	43	1.3	2.5	4.2	
2D-square (6 s period)	123	67	44	1.1	2.2	3.6	
Cube MP4D (6 s period)	1066	600	405	1.1	2.1	3.4	
XCAT (6 s period)	954	550	381	1.0	1.9	3.1	

gamma-index comparison between planned and delivered dose and display the results, or even manual intervention if deemed necessary.

The mean reconstruction timeframe includes several procedures: (1) application of the motion model on the GUI, (2) cleaning of the 4D-DDS information to extrapolate the spot parameters, (3) sending the data package to the FDC, (4) generating a new CT and the dose reconstruction, and finally (5), dose transfer from GPU to CPU and back to the GUI. Most of these processes have a stable processing time; for example, generating a new CT and warping the dose back on the midP CT takes about 3 ms each, while the actual dose reconstruction time is affected by the number of spots.

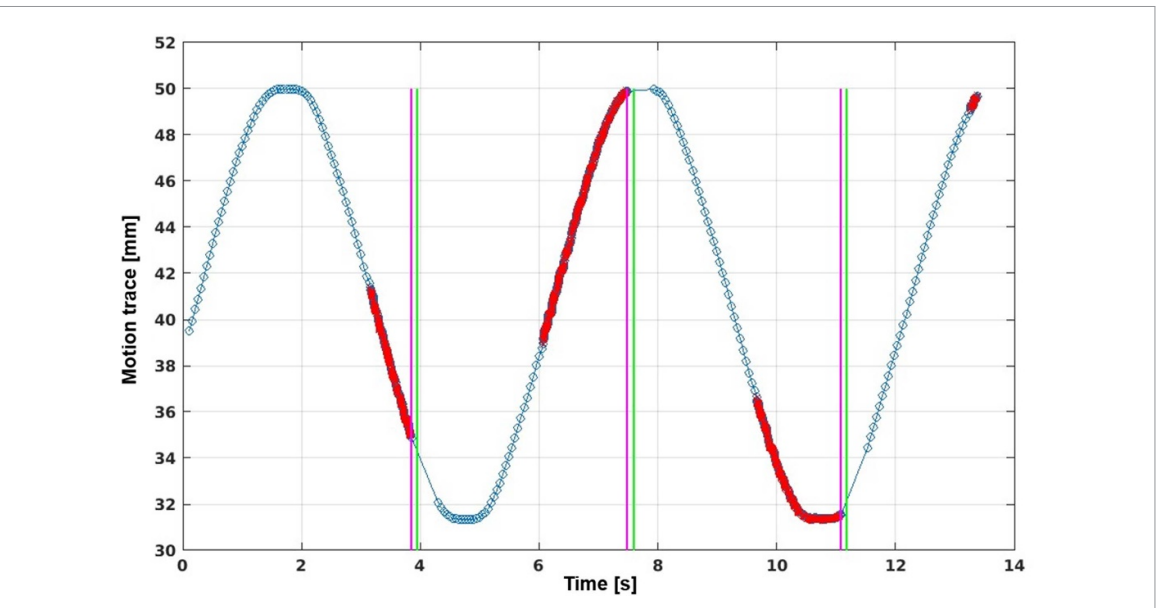


**Figure 6.** Delivery record with motion trace (blue line) and delivered spots (red crosses). The purple line shows when the GUI receives the iso-energy slice end event from the 4D-DDS and the green line when the reconstructed dose is ready to be displayed. The image refers to a range-ITV delivery.

The maximum recorded number of spots is 319, for the cube MP4D plan, with a processing time of 118 ms, significantly lower than the about 2 s needed by the synchrotron at CNAO to accelerate particles for the next energy. Moreover, all the reconstructions have been performed in less than 150 ms, always smaller than the triggering time window.

#### 4. Discussion

We proposed a framework that integrates real-time motion modeling and treatment verification to manage irregular motion scenarios. By coupling CNAO's OTS and 4D-DDS with 5D-RIDOS, our system can generate virtual CTs and reconstruct the delivered dose in real-time for both regular and irregular motion. The goal is to provide automated feedback on treatment quality during delivery, without increasing personnel workload or disrupting an already tight workflow. The algorithm detects machine errors and the impact of motion irregularities, allowing adjustments for subsequent fractions or even between beams. This is crucial for daily adaptive particle therapy (Albertini *et al* 2024).

Some previous systems (Duetschler *et al* 2023, Steinsberger *et al* 2021) address the issue of irregular motion and how to estimate the impact on the accuracy of the treatment. However, these are all performed *a posteriori* and, to our knowledge, they are not fully integrated into a clinical system as 5D-RIDOS. A critical factor in this regard is the synchronization of motion detection and delivery timings, which can be challenging if run on independent, closed systems.

The non-regularity in the patients' motion has been proven to be one of the most detrimental factors on target coverage and increased OAR exposure (Meschini *et al* 2022, Mastella *et al* 2020). In particular, Meschini *et al* (2022) report no significant inter-fraction nor cycle-to-cycle variations in the target coverage for pancreas patients treated at CNAO with gating. However, one patient exhibiting larger tumor displacement (12.16 mm) experienced a 17% cycle-to-cycle reduction of D<sub>95%</sub>. Mastella *et al* (2020), in their phantom study, proved a maximum under-dosage of 28.1% for 20 mm amplitude motion with 50% intra-fraction variations, for an ungated intensity modulated proton therapy plan, robustly optimized in 4D.

Our framework successfully generated accurate virtual CTs using the motion model, showing strong agreement with the ground-truth CTs, validating the model's accuracy. Building on this, 5D-RIDOS performs dose reconstructions on the generated volumes, assessing the impact of residual and irregular motion compared to a 4DCT-based approach (section 3.2). Although the setup featured a direct one-to-one correlation between target and marker motion, not representative of real patient anatomy, the motion model also performed reliably in more realistic scenarios (Fassi *et al* 2015).

From a clinical perspective, one of the main strengths of the proposed approach is that it relies on systems already available in routine practice. The 4DCT is standard imaging for moving patients, and the

OTS used to drive the model is currently employed at CNAO for patient alignment. This ensures compatibility with existing workflows, facilitating future clinical implementation without major infrastructural changes. Nonetheless, some limitations must be acknowledged. The motion model (Fassi *et al* 2015) is updated before each treatment fraction based on the daily CBCT, via a non-rigid registration to the midP CT. However, CBCT acquisition may suffer motion-related blurring and image artifacts, potentially reducing the model fidelity. Although not investigated in this study, available deep-learning mitigation strategies (Rusanov *et al* 2022) may help address these limitations and improve robustness in clinical use.

The fast dose reconstruction capability of 5D-RIDOS enables real-time dose monitoring by reconstructing and comparing the delivered dose with the planned one within the inter-spill time, as demonstrated in section 3.3. This allows the system to act as a dose monitoring tool, identifying if and when replanning is necessary. Based on this monitoring, adaptive replanning of subsequent fractions can be performed in an informed manner, re-optimizing the remaining treatment to meet the original planning objectives. Furthermore, adaptation can also occur between individual fields within a single fraction, applying a similar informed re-optimization approach. Thanks to its high computational speed, 5D-RIDOS has the potential to support even more advanced, real-time adaptive strategies. Recent papers on fast re-optimization (Oud *et al* 2024), in particular dose restoration approaches (Miyazaki *et al* 2023), suggest that real-time adaptive therapy could be integrated into 5D-RIDOS. With GPU parallelism, spot weights could be optimized based on delivery status, and the system could be easily integrated with the DDS-RIDOS complex system for additional benefits.

The current FDC implementation uses an analytical pencil-beam algorithm (Russo *et al* 2015), which cannot capture the real physics of particles in complex tissues. In particular, the dose calculation relies on LUTs precomputed in water and assumes water equivalence in the lateral direction of beam propagation. While this is acceptable in homogeneous media, such simplifications may significantly affect accuracy with real patients. Indeed, more complex anatomies require a Monte Carlo algorithm (Mein *et al* 2019), but these are too slow for real-time carbon ion dose calculation. Deep-learning dose engines are advancing, especially for protons, offering Monte Carlo accuracy with processing times similar to 5D-RIDOS (Pastor-Serrano and Perkó 2022). However, these advancements have not yet been applied to carbon ion therapy due to the complexity of fragmentation and the need for RBE-weighted dose calculations. Nonetheless, there are ongoing studies in this direction (Quarz *et al* 2024), which will in the future replace our dose engine, alongside the CT reconstruction model, achieving Monte Carlo accuracy of a sub-second dose reconstruction, calculated on the estimated anatomy of the moment.

The current CNAO OTS setup has a 30 ms latency with 4D-DDS, affecting spot assignment and residual motion estimation. To quantify the impact of this latency, we developed a deep learning model able to predict the motion trace 150 ms in advance. Reconstructed doses based on the predicted motion showed results consistent with the real motion traces, demonstrating the minimal impact of the latency.

A further test of the system, necessary before a real application on patients, would be on a heterogeneous and anthropomorphic phantom, such as Perrin et~al~(2017). The tissue heterogeneities and more complex motion will most likely cause a reduction in the precision of the dose reconstruction. If needed, this effect can be mitigated by employing sub-pencils, at the cost of longer processing times (Yang et~al~2020). Moreover, to further evaluate the framework's robustness under more diverse clinical scenarios, the impact of irregular motion should also be assessed using alternative treatment strategies beyond gating, such as ITV and regating plans.

An application for cyclotron-based proton therapy has not been tested yet, but would require minor adaptations of the workflow to mitigate the missing beam pauses, and likely lead to a slight delay, in the order of seconds, of the displayed results relative to the delivery.

The system has been tested with carbon ions but it can work with protons or other ions as well, as long as it is commissioned with the correct 3D-LUTs. In the case of protons, due to the larger lateral spread, the current raytracing algorithm might be inadequate and sub-pencil beams might be necessary, which can lead to an increase in the processing time. As currently only a fraction of the beam pause is used for dose reconstruction, the complexity of the algorithm can be significantly increased while still keeping the real-time capability.

The accuracy of 5D-RIDOS depends on the precision of the available imaging, and therefore provides only one of the necessary building blocks of successful online adaptive therapy. As shown by Meschini *et al* (2021), the motion model is accurate for 4D MRI sequences, so an integration with a future MR-particle therapy system might be ideal (Hoffmann *et al* 2020). Any type of in-room imaging made available to

5D-RIDOS would greatly improve the value of the supplied information. In this context, it can also provide instant dose assessment for newly available images to facilitate the acceptance of adaptive particle therapy.

#### 5. Conclusions

We developed a real-time framework that integrates a motion model with 4D-dose reconstruction, enabling accurate assessment of delivered dose under both regular and irregular motion conditions. Both the dose reconstruction algorithm and the motion model used for virtual CT generation proved to be accurate and robust within a fully clinical setup.

By continuously accounting for motion-induced anatomical changes, the system enables the identification of discrepancies between planned and delivered doses during treatment, which can support adaptation between fractions or even between beams. Its timing performance also opens perspectives for real-time adaptive treatments.

#### Data availability statement

All data that support the findings of this study are included within the article (and any supplementary information files).

#### Acknowledgment

This study has been funded by the European Union's Horizon 2020 research and innovation program under the Marie Sklodowska-Curie Grant RAPTOR—Real-Time Adaptive Particle Therapy of Cancer, Grant Agreement No. 966956. This work was partially carried on within the SIG\_PNR project of the Istituto Nazionale di Fisica Nucleare under the supervision of the Commissione Scientifica Nazionale 5.

#### Appendix A. Motion model construction

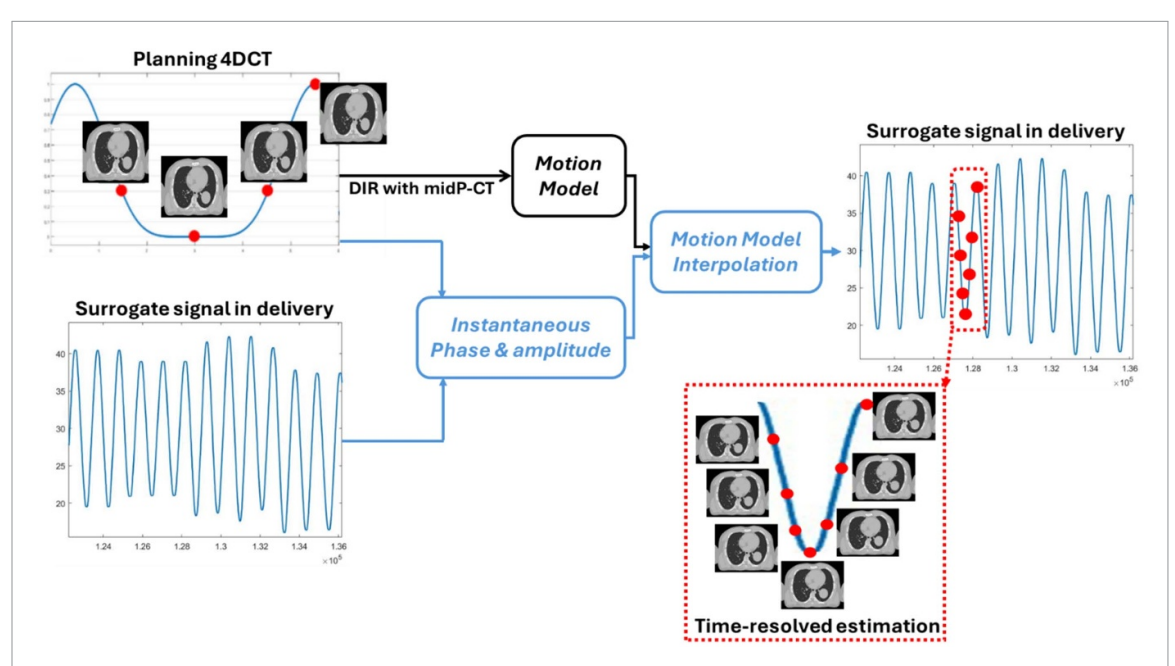


**Figure A.** Schematic representation of the motion model (Fassi *et al* 2015) used in this study. The process begins with the generation of the midP-CT (a time-averaged volume over the planning 4DCT), which is then deformed across all 4DCT phases to construct the motion model, represented as a set of deformable vector fields (DVFs). During treatment, planning and delivery signals are continuously compared, and a Hilbert transform is applied to determine the instantaneous phase and amplitude parameters. These parameters are then used to interpolate the DVFs, enabling the generation of updated virtual CT volumes throughout the entire delivery signal.

#### Appendix B. 5D-RIDOS workflow

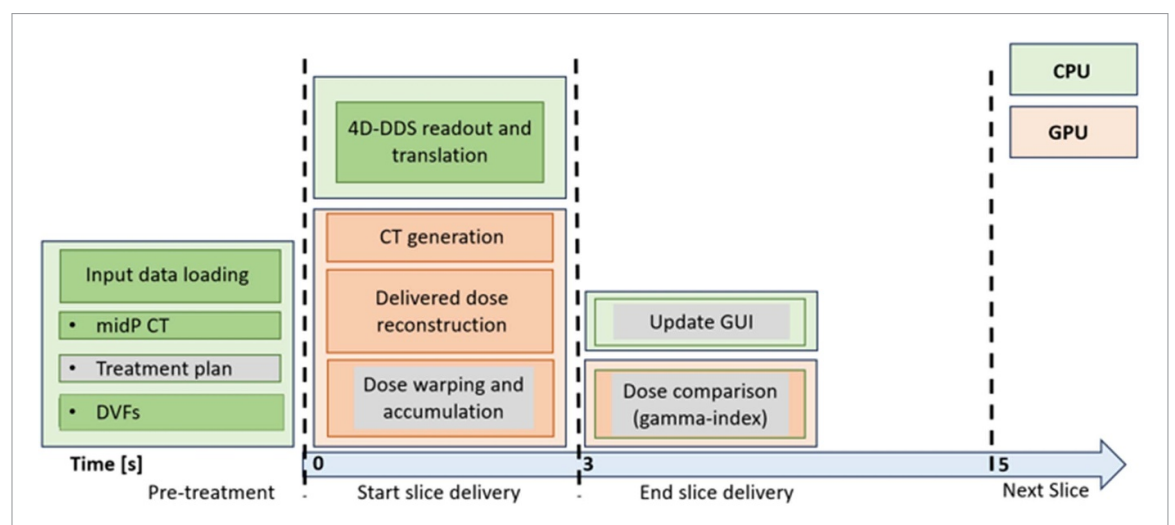


**Figure B.** Workflow of the system operations divided with respect to treatment time. Pre-treatment, the system loads the midP CT, the treatment plan, and the deformable vector fields (DVFs) for generating the updated anatomy of the patient and reconstructing the dose. During each iso-energy slice delivery, the system receives spot parameters and the OTS-derived motion trace from the 4D-DDS, generates a new CT, and reconstructs the delivered dose. At the end of the delivery of each iso-energy slice, the system updates the GUI which runs an independent gamma-index analysis between planned and delivered doses. The procedure is repeated until the end of treatment. The boxes in green report operations performed on the CPU, while in orange on the GPU. The boxes in gray involve operations already described and maintained as in Giordanengo *et al* (2019) and Galeone *et al* (2024).

#### **ORCID** iDs

C Galeone © 0009-0006-4048-1728
A Nakas © 0009-0000-2813-0972
M Donetti © 0000-0001-7489-6274
M C Martire © 0009-0006-5331-9463
F M Milian © 0000-0002-5588-1672
A Vignati © 0000-0001-8137-9080
M Durante © 0000-0002-4615-553X
S Giordanengo © 0000-0001-6347-1182
C Graeff © 0000-0002-5296-7649

#### References

Albertini F et al 2024 First clinical implementation of a highly efficient daily online adapted proton therapy (DAPT) workflow Phys. Med. Biol. 69 215030

Barker Jr J L et al 2004 Quantification of volumetric and geometric changes occurring during fractionated radiotherapy for head-and-neck cancer using an integrated CT/linear accelerator system Int. J. Radiat. Oncol. Biol. Phys. 59 960–70

Bert C *et al* 2008 Quantification of interplay effects of scanned particle beams and moving targets *Phys. Med. Biol.* **53** 2253–65 Bert C and Durante M 2011 Motion in radiotherapy: particle therapy *Phys. Med. Biol.* **56** R113–R44

Bertholet J et al 2019 Real-time intrafraction motion monitoring in external beam radiotherapy Phys. Med. Biol. 64 15TR01

Choi K, Mein S B, Kopp B, Magro G, Molinelli S, Ciocca M and Mairani A 2018 FRoG—a new calculation engine for clinical investigations with proton and carbon ion beams at CNAO *Cancers* 10 1–14

Ciocca M et al 2016 Commissioning of the 4-D treatment delivery system for organ motion management in synchrotron-based scanning ion beams *Phys. Med.* **32** 1667–71

Den Otter L A 2020 *et al* Investigation of inter-fraction target motion variations in the context of pencil beam scanned proton therapy in non-small cell lung cancer patients *Med. Phys.* 47 3835–44

Dhont J et al 2018 The long- and short-term variability of breathing induced tumor motion in lung and liver over the course of a radiotherapy treatment Radiother. Oncol. 126 339–46

Donetti M, Giordanengo S, Graeff C, Lis M, Milian F M, Pullia M, Steinsberger T, Vignati A and Rossi S 2021 Current and future technologies of the cnao dose delivery system *IEEE Instrum. Meas. Magn.* 24 61–69

Duetschler A et al 2023 A motion model-guided 4D dose reconstruction for pencil beam scanned proton therapy Phys. Med. Biol. 68 115013

Durante M and Loeffler J S 2010 Charged particles in radiation oncology Nat. Rev. Clin. Oncol. 7 37-43

Fassi A, Seregni M, Riboldi M, Cerveri P, Sarrut D, Ivaldi G B, de Fatis P T, Liotta M and Baroni G 2015 Surrogate-driven deformable motion model for organ motion tracking in particle radiation therapy *Phys. Med. Biol.* **60** 1565–82

Fattori G et al 2014 Commissioning of an integrated platform for time- resolved treatment delivery in scanned ion beam therapy by means of optical motion monitoring Technol. Cancer Res. Treat. 13 517–28

Galeone C et al 2024 Real-time delivered dose assessment in carbon ion therapy of moving targets Phys. Med. Biol. 69 205001

Giordanengo S et al 2015 The CNAO dose delivery system for modulated scanning ion beam radiotherapy Med. Phys. 42 263–75

Giordanengo S et al 2019 RIDOS: a new system for online computation of the delivered dose distributions in scanning ion beam therapy Phys. Med. 60 139–49

Graeff C 2014 Motion mitigation in scanned ion beam therapy through 4D-optimization Phys. Med. 30 570-7

Grassberger C, Dowdell S, Sharp G and Paganetti H 2015 Motion mitigation for lung cancer patients treated with active scanning proton therapy Med. Phys. 42 2462–9

Hoffmann A et al 2020 MR-guided proton therapy: a review and a preview Radiat. Oncol. 15 1-13

Lawler M et al 2023 European Groundshot—addressing Europe's cancer research challenges: a Lancet Oncology Commission Lancet Oncol. 24 e11–e56

Lis M, Donetti M, Newhauser W, Durante M, Dey J, Weber U, Wolf M, Steinsberger T and Graeff C 2020 A modular dose delivery system for treating moving targets with scanned ion beams: performance and safety characteristics, and preliminary tests *Phys.* Med. 76 307–16

Lomax A J 2020 Proton therapy special feature: review article myths and realities of range uncertainty Br. J. Radiol. 93 1-9

Mastella E et al 2020 4D strategies for lung tumors treated with hypofractionated scanning proton beam therapy: dosimetric impact and robustness to interplay effects Radiother. Oncol. 146 213–20

MATLAB 2018b I. The MathWorks

Matsuo Y et al 2014 Evaluation of dynamic tumour tracking radiotherapy with real-time monitoring for lung tumours using a gimbal mounted linac Radiother. Oncol. 112 360–4

Meijers A, Jakobi A, Stützer K, Guterres Marmitt G, Both S, Langendijk J A, Richter C and Knopf A 2019 Log file-based dose reconstruction and accumulation for 4D adaptive pencil beam scanned proton therapy in a clinical treatment planning system: implementation and proof-of-concept *Med. Phys.* 46 1140–9

Mein S *et al* 2019 Dosimetric validation of Monte Carlo and analytical dose engines with raster-scanning <sup>1</sup>H, <sup>4</sup>He, <sup>12</sup>C, and <sup>16</sup>O ion-beams using an anthropomorphic phantom *Phys. Med.* **64** 123–31

Mein S et al 2024 Particle arc therapy: status and potential Radiother. Oncol. 199 110434

Meschini G et al 2021 An MRI framework for respiratory motion modelling validation J. Med. Imaging Radiat. Oncol. 65 337-44

Meschini G et al 2022 Time-resolved MRI for off-line treatment robustness evaluation in carbon-ion radiotherapy of pancreatic cancer Med. Phys. 49 2386–95

Miyazaki K et al 2023 Deformed dose restoration to account for tumor deformation and position changes for adaptive proton therapy Med. Phys. 50 675–87

Nakas A et al 2024 Modelling strategies to enable time-resolved volumetric imaging Imaging in Particle Therapy: Current Practice and Future Trends (IOP Publishing) pp 9-1–9-20

Oud M, Breedveld S, Rojo-Santiago J, Giżyńska M K, Kroesen M, Habraken S, Perkó Z, Heijmen B and Hoogeman M 2024 A fast and robust constraint-based online re-optimization approach for automated online adaptive intensity modulated proton therapy in head and neck cancer *Phys. Med. Biol.* 69 075007

Pakela J M, Knopf A, Dong L, Rucinski A and Zou W 2022 Management of motion and anatomical variations in charged particle therapy: past, present, and into the future *Front. Oncol.* 12 1–16

Parodi K, Yamaya T and Moskal P 2023 Experience and new prospects of PET imaging for ion beam therapy monitoring Z. Med. Phys. 33 22–34

Pastor-Serrano O and Perkó Z 2022 Millisecond speed deep learning based proton dose calculation with Monte Carlo accuracy Phys. Med. Biol. 67 105006

Perrin R L et al 2017 An anthropomorphic breathing phantom of the thorax for testing new motion mitigation techniques for pencil beam scanning proton therapy *Phys. Med. Biol.* 62 2486–504

Persoon L C G G, Podesta M, van Elmpt W J C, Nijsten S M J J G and Verhaegen F 2011 A fast three-dimensional gamma evaluation using a GPU utilizing texture memory for on-the-fly interpolations *Med. Phys.* 38 4032–5

Quarz A, Gregorio A D, Franciosini G, Schiavi A, Perko Z, Volz L, Patera V, Durante M and Graeff C 2024 An AI dose engine for fast carbon ion treatment planning *Int. J. Part. Ther.* 12 100222

Riboldi M, Orecchia R and Baroni G 2012 Real-time tumour tracking in particle therapy: technological developments and future perspectives *Lancet Oncol.* 13 e383–e91

Richter D, Schwarzkopf A, Trautmann J, Krämer M, Durante M, Jäkel O and Bert C 2013 Upgrade and benchmarking of a 4D treatment planning system for scanned ion beam therapy *Med. Phys.* 40 1–17

Rusanov B, Hassan G M, Reynolds M, Sabet M, Kendrick J, Rowshanfarzad P and Ebert M 2022 Deep learning methods for enhancing cone-beam CT image quality toward adaptive radiation therapy: a systematic review *Med. Phys.* 49 6019–54

Russo G et al 2015 A novel algorithm for the calculation of physical and biological irradiation quantities in scanned ion beam therapy: the beamlet superposition approach Phys. Med. Biol. 61 183–214

Sanford N N et al 2019 Protons versus photons for unresectable hepatocellular carcinoma: liver decompensation and overall survival Int. J. Radiat. Oncol. Biol. Phys. 105 64–72

Segars W P, Mahesh M, Beck T J, Frey E C and Tsui B M W 2008 Realistic CT simulation using the 4D XCAT phantom *Med. Phys.* 35 3800–8

Siddon R L 1985 Fast calculation of the exact radiological path for a three-dimensional CT array Med. Phys. 12 252-5

Steinsberger T, Alliger C, Donetti M, Krämer M, Lis M, Paz A, Wolf M and Graeff C 2021 Extension of RBE-weighted 4D particle dose calculation for non-periodic motion *Phys. Med.* **91** 62–72

Steinsberger T, Donetti M, Lis M, Volz L, Wolf M, Durante M and Graeff C 2023 Experimental validation of a real-time adaptive 4D-optimized particle radiotherapy approach to treat irregularly moving tumors *Int. J. Radiat. Oncol. Biol. Phys.* 115 1257–68 Trnkova P *et al* 2023 A survey of practice patterns for adaptive particle therapy for interfractional changes *Phys. Imaging Radiat. Oncol.* 26 100442

Vingelmann P and Fitzek F H P (NVIDIA) 2022 CUDA release: 11.6

Werner J et al 2024 Stopping power and range estimations in proton therapy based on prompt gamma timing: motion models and automated parameter optimization Phys. Med. Biol. 69 14NT02

Yang J, He P, Wang H, Sun G, Zheng H and Jia J 2020 An improved beam splitting method for intensity modulated proton therapy *Phys. Med. Biol.* 65 185015

Yoganathan S, Maria Das K J, Agarwal A and Kumar S 2017 Magnitude, impact, and management of respiration-induced target motion in radiotherapy treatment: a comprehensive review *J. Med. Phys.* 42 101–15

Zhang Y et al 2023 A survey of practice patterns for real-time intrafractional motion-management in particle therapy Phys. Imaging Radiat. Oncol. 26 100439